Fiber tracking in q-ball fields using regularized particle trajectories

M. Perrin[1,3], C. Poupon[1,3], Y. Cointepas[1,3], B. Rieul[1,3], N. Golestani[1,2], C. Pallier[1,2], D. Rivière[1,3], A. Constantinesco[4], D. Le Bihan[1,3], and J.-F. Mangin[1,3]

[1] Service Hospitalier Frédéric Joliot, CEA, 91401 Orsay, France
perrin@shfj.cea.fr,http://brainvisa.info
[2] INSERM U562 Cognitive Neuro Imaging, Orsay, France
[3] Institut Fédératif de Recherche 49 (Imagerie Neurofonctionnelle), Paris
[4] CHU Hautepierre, Strasbourg

Abstract. Most of the approaches dedicated to fiber tracking from diffusion-weighted MR data rely on a tensor model. However, the tensor model can only resolve a single fiber orientation within each imaging voxel. New emerging approaches have been proposed to obtain a better representation of the diffusion process occurring in fiber crossing. In this paper, we adapt a tracking algorithm to the q-ball representation, which results from a spherical Radon transform of high angular resolution data. This algorithm is based on a Monte-Carlo strategy, using regularized particle trajectories to sample the white matter geometry. The method is validated using a phantom of bundle crossing made up of haemodialysis fibers. The method is also applied to the detection of the auditory tract in three human subjects.

1 Introduction

Brownian motion of water molecules in brain white matter is disturbed by the fiber bundle microscopic structure. Therefore, the anisotropy of the molecule displacements embeds information about the fiber bundle orientations. Hence, diffusion MRI, which probes these water molecule displacements, provides a way to detect the main bundles and to map the large scale connectivity of the brain.

A lot of methods have been proposed for this purpose. Most of them rely on a tensor model of the water diffusion process (Diffusion Tensor Imaging, DTI) [1, 15]. This model, however, is too simple to represent the complex diffusion process occurring in voxels filled by fiber crossing. More sophisticated models have been recently introduced to overcome these difficulties [22, 8, 16]. They usually aim at explaining the MR signal as a mixture of tensor models. They provide convincing results in some crossing areas, but lack the versatility required to untangle any complex diffusion pattern (fan-shaped bundle, bending fibers, kissing fibers, etc.). Therefore, another strategy consists in using iconic representations of the diffusion process, namely an image for each voxel. This point of view alleviates the risk of misinterpreting the MR data because of the narrowness of the model.

Diffusion Spectrum Imaging (DSI), which provides for each voxel a 3D image of the water displacement probability distribution, is the most attractive solution [25, 12]. Unfortunately DSI is based on sampling the 3D Fourier space of the water displacement distribution, which requires large pulsed field gradients and time-intensive acquisition.

Therefore DSI can not be used in clinical situations. However, it has been shown recently that the orientation distribution function (ODF) of this probability distribution can be reconstructed from high angular resolution diffusion imaging (HARDI) using a spherical tomographic inversion called the Funk-Radon transform, also known as the spherical Radon transform [21]. This technique called q-ball imaging could resolve intravoxel white matter fiber crossing as well as white matter insertions into cortex [23].

In this paper, we propose a new algorithm to infer fiber bundles from q-ball imaging data. This algorithm combines the idea of performing a probabilistic tractography [4, 3, 16] with regularization of the curvature of the particle trajectories used to sample the white matter organization [17, 24, 13, 5]. The method is first validated with a phantom of fiber crossing made up of haemodialysis fibers. Then, the method is successfully applied to the detection of the auditory tract in 3 human subjects. This tract can not be detected with the standard DTI-based streamline method [14, 6, 2] because of its crossing with a large orthogonal bundle.

2 Method

2.1 QBall imaging

The QBall model has been introduced by David Tuch in 2002 because performing routine DSI acquisition was too difficult [20]. The MR diffusion signal E is related to the diffusion function P by the Fourier relation $P = F[|E(q)|]$ where q is the diffusion wave-vector. The radial projection of the diffusion function is called the diffusion ODF and is defined as $\psi(u) = \int_0^\infty P(ru)dr$, where u is the unit direction vector. Given a sampling of E on a sphere (HARDI), David Tuch demonstrated that the spherical Radon transform or Funk-Radon Transform (FRT) provides a good approximation of this ODF. Let us consider a function p(w) on a sphere where w is the unit direction vector: for a given direction of interest u, the FRT is defined as the integral over the corresponding equator.

$$S[u] = \int_{w \perp u} p(w)dw. \tag{1}$$

David Tuch demonstrated that the FRT of E evaluated at a particular radius q' can be written in cylindrical coordinates as :

$$S_{q'}[E] = 2\pi q' \int P(r, \theta, z) J_0(2 * \pi * q' r) r dr d\theta dz \tag{2}$$

where J_0 is the 0^{th} order Bessel Function. If we replace this Bessel function by a delta function, $\delta(r)$, then we obtain the radial projection ODF exactly. Therefore, due to the Fourier relationship between the diffusion MR signal and the diffusion function, we can exploit this finding to measure the displacement probability in a particular direction by simply summing the diffusion MR signal along an equator around that direction [23, 21]. Q-ball field is the result of this summation computed voxel by voxel.

In the following, q-ball data are visualised according to the following rules. Each q-ball is represented by a spherical mesh. Each node of the mesh is moved outward according to the water molecule displacement probability. In order to maximize the

information provided by this deformation process, this motion is computed as $(p - min_S(p))/(max_S(p) - min_S(p))$, where p is the node probability and S the sampled sphere of the current voxel. To improve visualisation further, each node is given a color related to its orientation relative to the image axis: red for x axis, green for y axis and blue for z axis, interpolated in between.

2.2 Fiber direction and ODF

Due to the mathematical approximation mentioned above, the q-ball-based ODF does not match exactly the actual ODF. Moreover, the relationship between the diffusion ODF and the fiber ODF is an open issue governed for instance by the link between the physics of diffusion and some biophysical properties of the tissue such as cell membrane permeability or free diffusion coefficients for the different cellular compartments. This issue corresponds to a crucial research program for the community of diffusion imaging. This program, however, needs time to deliver some answers, which should not stop the development of tracking algorithms. These algorithms, indeed, have the possibility to use contextual knowledge, namely the neighborhood of a voxel, in order to tackle locally the inverse problem: which geometry of fiber can explain such q-ball data. Therefore, in the following, we assimilate the diffusion ODF with the fiber ODF, but the relationship could be refined in the future. One key issue, for instance, when dealing with q-ball imaging will be the optimal choice of the radius q' of the HARDI acquisition. Increasing q', indeed, sharpens the Bessel kernel and increases the ability to resolve distinct diffusion peaks but at the cost of a lower signal to noise ratio.

2.3 Probabilistic tracking and curvature regularization

The simplest approaches for fiber tracking, which are based on DTI, are variants of the "streamline" method. The eigenvector of the tensor associated with the highest eigenvalue is supposed to provide the local fiber direction. Then this local direction is followed step by step in order to build 3D trajectories supposed to correspond to the bundles [14, 6, 2]. Unfortunately, in case of partial volume (fiber crossing), the diffusion ellipsoid associated to the tensor may be a disk or a sphere. In such cases, the first eigenvector indicates a spurious fiber direction leading to false fork of the tracking process.

Various approaches have been proposed to reduce the bad influence of ambiguous tensors. They all involve the use of the entire tensor information. For instance the tensor is used in [26, 9] to deflect the estimated fiber trajectory leading to the reconstruction of "tensorlines". Another approach considers the tensor field as a Riemannian manifold and the fibers as some geodesics of this manifold [10]. Using a regularization point of view leads to define the fibers as a trade-off between high diffusion along fibers and low curvature constraints [17]. The tensor field can also feed a model of uncertainty on the fiber orientation used to perform Monte-Carlo estimations of the connectivity [4, 3] or probabilistic tracking [5].

All these approaches perform better than the simple streamline idea. However, when getting close to the cortex, they get in touch with large areas of crossing fibers where the reliability of the results drop down. In such areas, the tracking problem becomes

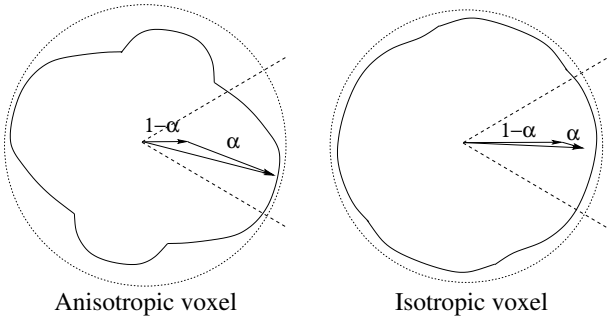

Fig. 1. *The normalized standard deviation of the q-ball provides a measure of anisotropy α, that is used to weight the influence of the q-ball on the particle trajectories.*

ill-posed because of the poor representation of the diffusion process provided by the tensor. There is now a consensus that higher angular resolution data like HARDI is required to untangle such crossing. New approaches are then needed to infer information on the fiber orientation from such data. The multi-tensor point of view converts HARDI into a short list of fiber directions for each voxel that can be used to develop tracking approaches [16]. A weakness of this strategy stems from the potential failures of the process leading to this list, either a standard fitting procedure [22] or more sophisticated approaches from information theory [8]. The q-ball approach, which converts directly the diffusion data into a fiber ODF, overcomes this difficulty. Therefore, this data representation seems the perfect candidate for developing Monte-Carlo estimation of white matter geometry. In the following, we describe such an approach where this geometry is sampled using regularized particle trajectories.

Like most approaches, our method requires a Region of Interest (ROI) as input. Each voxel of this ROI is spatially sampled in order to define the starting points of n particles. These particles move inside a continuous q-ball field defined by linear interpolation. Each particle is endowed with an initial speed in the direction of the q-ball maximum. Then, each particle moves with constant speed according to a simplistic sampling scheme: let us note $p(i)$ the location of the particle at time i, and $\overrightarrow{v(i)}$ the direction of the particle speed at time i:

$$p(i+\delta t) = p(i) + \overrightarrow{v(i)} * \delta t \tag{3}$$

The behaviour of the particle speed direction can be understood from a simple mechanical analogy: at each step of the trajectory sampling, the new speed $\overrightarrow{v(i+\delta t)}$ results from a trade-off between inertia ($\overrightarrow{v(i)}$) and a force stemming from the local q-ball ($\overrightarrow{v_q}$):

$$\overrightarrow{v(i+\delta t)} = \alpha \overrightarrow{v_q} + (1-\alpha)\overrightarrow{v(i)} \tag{4}$$

where α is a parameter ranging between 0 and 1 that will be described latter. The orientation $\overrightarrow{v_q}$ of the force acting on the particle is chosen randomly inside a half cone defined from the incident direction $\overrightarrow{v(i)}$. The probability distribution driving this sampling cor-

responds to the restriction of the q-ball to this half cone. Therefore, the maximum of the q-ball inside the half cone has the highest probability.

The parameter α is the standard deviation of the q-ball normalized by its maximum in the field. Hence, this weight depends on the location in the q-ball field. In fact α is a measure of anisotropy [7]. For isotropic voxels, α parameter is small and the algorithm favours incident orientation; while for anisotropic voxels, α parameter is large and the algorithm favours q-ball distribution (see Fig. 1).

The particle trajectory regularization depends on three parameters:

1. the half-cone angle is used to discard the diffusion peaks leading to high curvature of the trajectory. In the following, the cone angle defined from the cone axis is 30 degrees.
2. the q-ball standard deviation (α parameter) tunes the weight of inertia.
3. the constant sampling δt provides another level of tuning: increasing the trajectory sampling decreases curvature regularization. In all the following, δt is set such as the particles do a 0.5 mm move at each iteration.

In this paper, the influence of these ad hoc parameters is not explored. The algorithm proposed in this paper, indeed, aims mainly at studying the inner organization of the q-ball field and its links with the bundle organization. It is too early to address the optimal tuning of such parameters.

The particles propagate throughout a mask computed from the T2 image. Trajectories stop only when they leave the mask. After the propagation, a postprocessing can be applied to keep only the reliable part of a bundle. After selection of a set of particle trajectories, for instance using a second ROI, a meter is used for each voxel accounting for the number of particles which go through that voxel. Then, the trajectories crossing some voxels whose meter is under a given threshold are discarded as non significant.

3 Fiber crossing phantom

The lack of knowledge about the white matter organization of the human brain is a huge handicap for the community developing fiber tracking algorithms. Considering the complexity of the MR diffusion signal, it is rather difficult to validate such algorithms using only simulated data. Therefore, the development of phantoms with known geometry is in our opinion crucial for a better understanding of the algorithm behaviours [12].

For this purpose, we have designed a phantom corresponding to two intersecting fiber bundles. It consists of sheets of parallel haemodialysis Fibers (Gambro, Polyflux 210 H) with an inner diameter of 200 micrometers and an outer diameter of 250 micrometers. Sheets of two different orientations intersecting at 90 degrees were stacked on each other in an interleaved fashion [12]. Crossing thickness is above 2cm. Fibers are suspended and hold by two arms as seen in Fig. 2. Fibers are permeable to water. They are dived in pure water mixed with gadolinium.

We performed MRI acquisitions with a 1.5 Tesla magnet (Signa, General Electrics) with maximal gradient intensity of 40 mT m^{-1}. Acquisitions were performed with Spin echo EPI sequence and Stejskal and Tanner diffusion gradient [19]: b value is 700

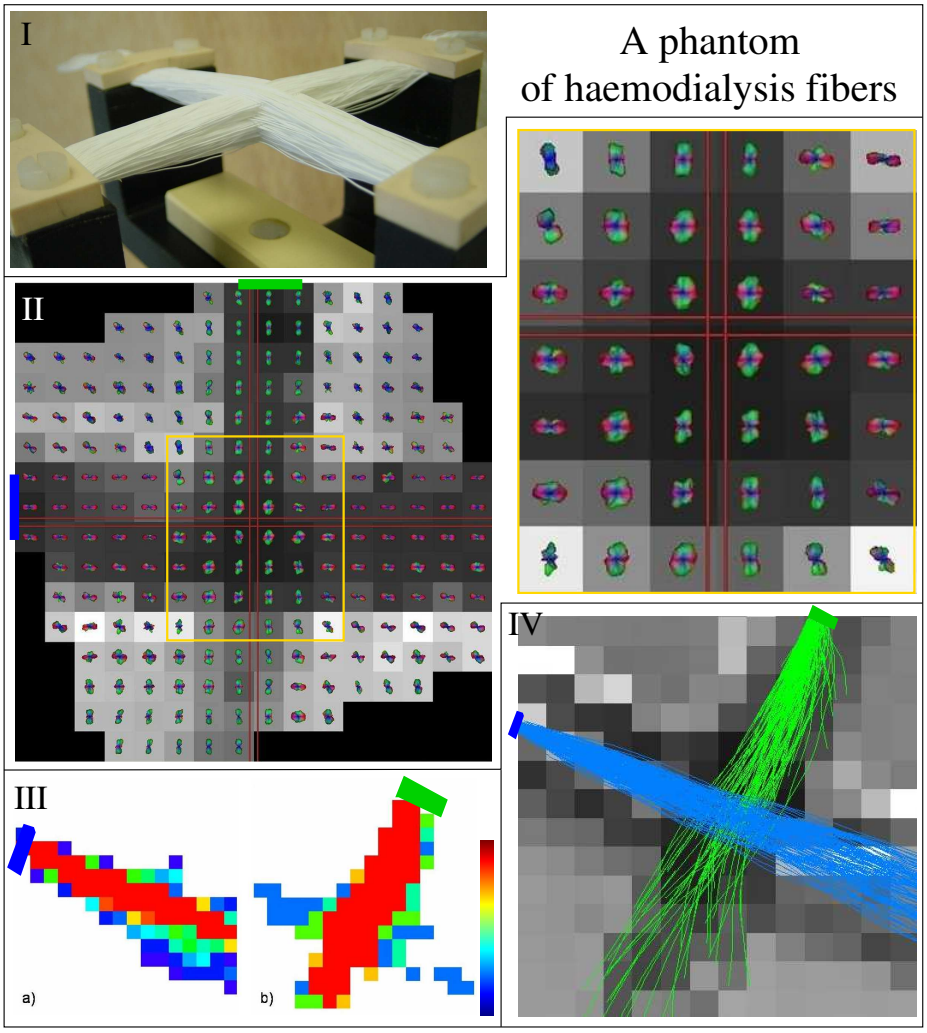

Fig. 2. *I: A phantom of fiber crossing. II: A slice of the 512 directions q-ball acquisition with a zoom on the crossing area. q-balls are superimposed on a T2-weighted MR image whose intensity is related to water amount. q-balls and MR data have been slightly rotated in order to simplify the reading of the q-ball 3D color code. Green and blue rectangles denote the regions of interest at the origin of fiber tracking. III: Slices of the number of particles crossing each voxels at the end of the fiber sampling (left: blue bundle, right: green bundle). IV: Trajectories selected by a threshold on the particle density map for each bundle. A T2-weighted slice of the phantom crossing the bundles is used as background and hides some trajectories.*

s mm^{-2}, equivalent to 2000 s mm^{-2} for diffusion in brain white matter, 512 orientations of the diffusion gradient (HARDI), Matrix 64 x 64, In-plane voxel resolution 3.75 x 3.75 mm, Slice thickness 2.0 mm, TE 66.6 ms, TR 3000 ms, 1 shot, field of view

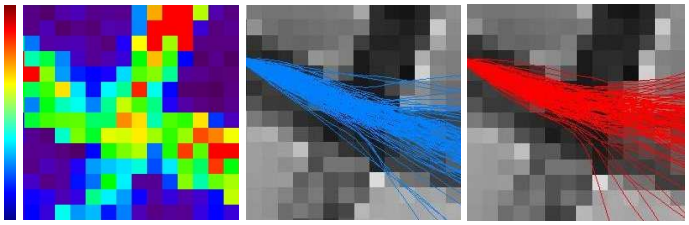

Fig. 3. Left*: a slice of the normalized standard deviation of the q-ball* (α)*.* **Middle***: particle trajectories in the initial q-ball field (T2-weighted image behind).* **Right***: particle trajectories in the field where the q-balls of the crossing area have been rotated around the z axis (20 degrees).*

24 cm. Spatial distortions of the diffusion-weighted images induced by Eddy currents were corrected before estimation of the q-ball field. This correction relies on a slice by slice affine geometric model and maximization of mutual information with the diffusion free T2-weighted image.

A slice of the q-ball field is shown in Fig. 2. Unfortunately, because of a difficult positioning of the phantom due to the shape of its container, the two crossing bundles are not parallel to the slice axes. To clarify the visualisation of the q-ball data based on color encoding, a rotation around the z-axis has been applied to the data before visualization. Then the orientation of each bundle corresponds to a pure color in the q-ball meshes (green and red). A zoom on the crossing area highlights the additional information provided by the q-ball compared to a tensor model. The diffusion peaks, however, would provide a better angular discrimination with higher b value (q').

For each bundle, the tracking algorithm is fed with a ROI made up of 3 voxels, using 3 x 130 particles. The particles propagate throughout a mask defined from the T2-weighted image. This mask corresponds to the part of the field of view including the artificial fibers. It was defined from a high threshold on intensity (the voxels including fibers contain less water, which leads to less signal), followed by a morphological closing in order to fill up spurious holes. A slice of the two resulting particle density maps is shown in Fig. 2. A threshold of 5 particles is applied to these maps in order to create a mask used to select reliable trajectories. The remaining trajectories do not include any spurious fork in the crossing area.

A second experiment was performed to check that the successful result was not only due to the fact that the phantom bundles have a straight geometry. With such a geometry, indeed, curvature regularization is sufficient for the particles to pass through the crossing area without trouble. For this second experiment, a 20 degree rotation around the z axis was applied to the q-balls of the crossing area corresponding to the zoom of Fig. 2. Then the tracking algorithm was triggered with the same set of particles as for the first experiment using first the initial q-ball field and second the modified field. However, the particles could propagate throughout the whole field (no mask) and no filtering of the trajectories was applied using the particle density map. The results shown in Fig. 3 prove that the curvature regularization does not prevent the particle to follow the rotated fiber direction indicated by the q-balls of the crossing area. This observation

means that the q-balls of the crossing area are anisotropic enough to oppose the particle inertia.

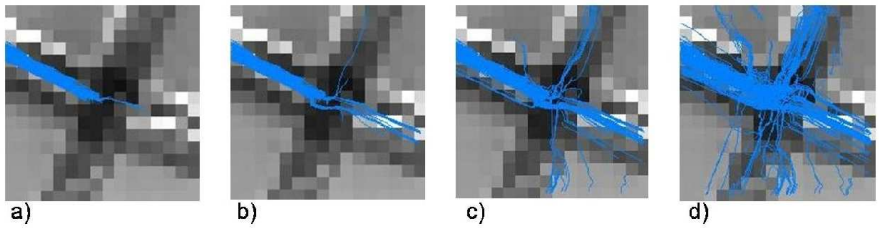

Fig. 4. *Streamline algorithm with different thresholds on the angle between two consecutive steps. a) 30 degrees, b) 60 degrees, c) 80 degrees d) 90 degrees*

A last experiment was performed to observe the behaviour of the streamline approach with the same data and the same ROIs. The algorithm was provided by brainVISA software (http://brainvisa.info). Each voxel of the ROI was spatially sampled in order to provide several starting points. The streamlines were sampled with 0.5mm steps. For each step, the tensor is estimated after linear interpolation of the 512 diffusion-weighted images and the streamline follows the direction of the main eigenvector. Streamlines are stopped by a threshold on the angle between two consecutive directions, namely a threshold on the streamline curvature. We performed the experiment with four different thresholds (30deg, 60deg, 80deg, 90deg). The results are shown in Fig. 4. With a 30deg threshold, the streamlines can not pass through the crossing area. Increasing the threshold allows the streamlines to go further, but the result is uncertain. When the streamlines remains inside the correct bundle, they include questionable high curvature parts. All these difficulties stem from the fact that the directions of the tensor main eigenvectors in the crossing area are not predictable.

4 Human brain

One of the bundles often used to illustrate the behaviour of tracking methods is the optic tract, which conveys information from the thalamus to the visual cortex in occipital lobe [6]. The optic tract is interesting for validation because it is one of the few well known bundles of brain architecture. A few other primary bundles like the pyramidal tract are used for the same purpose. Surprisingly, the auditory tract, which conveys information from the thalamus to the auditory cortex in temporal lobe, is usually absent from tracking reports. This bundle seems to be lost in a large crossing with orthogonal fibers. To study the potential of the approach described in this paper, the last experiment aims at detecting this primary tract.

The acquisitions used for this last experiment were not initially dedicated to q-ball methodology. Therefore, the angular resolution is low and the b-value is too small to get accurate information on the crossing geometry. Nevertheless, the q-ball approach can

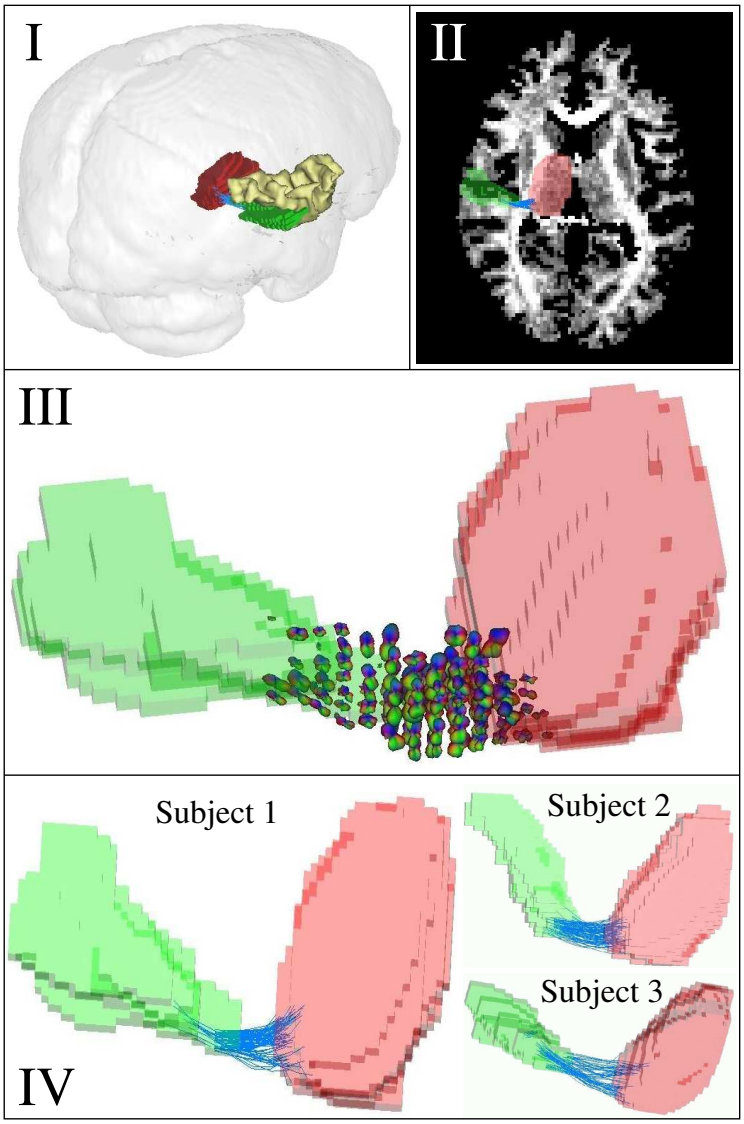

Fig. 5. *I: The two regions of interest (ROIs) used to define auditory tract are the thalamus (red) and Heschl gyrus (green), a good landmark of primary auditory area. The yellow object is the grey matter of the lateral fissure surrounding Heschl gyrus. The blue bundle, supposed to correspond to auditory tract, has been inferred from q-ball data. II: Intersection of the ROIs and of the tracked bundle with a slice of the anisotropy map (the parameter α mentioned in the text) computed inside the mask used for tracking. III: The q-balls of the voxels crossed by at least one particle trajectory linking the two ROIs. IV: the representation of the auditory tract obtained after thresholding the particle density map for the subject used above and for two other subjects.*

be used to analyze such data, which has been done for 3 different subjects. The acquisition parameters are the following: 41 diffusion gradient directions (HARDI), b value is 700 s mm^{-2}, Matrix 128 x 128, In-plane voxel resolution 1.875 x 1.875 mm, Slice thickness 2.0 mm, TE 66.6 ms, TR 2000 ms, single shot, FOV 24 cm. After correction of the spatial distortions induced by Eddy currents, the q-ball field was estimated using a tessellation of the sphere made up of 240 nodes. To improve further 3D visualization, a homothetic factor was applied to the q-ball meshes. This factor corresponds to the normalized standard deviation of the q-ball (α). Hence, anisotropic q-balls are larger than isotropic ones.

A white matter mask was used to prevent the particles to go through cortical folds. The process leading to this mask is the following. A low threshold was applied to the normalized standard deviation of the q-ball in order to get a first mask of anisotropic areas. This mask was used to compute the histogram of intensities of anisotropic areas in the T2-weighted image. A simple histogram analysis provides two thresholds allowing the definition of the white matter mask.

A good landmark of the primary auditory cortex is called Heschl gyrus, a small gyrus hidden in the temporal part of the lateral fissure [18, 11]. This gyrus and the thalamus have been drawn manually in the T2-weighted images (see Fig. 5). Each voxel of Heschl gyrus has been spatially sampled with 20 particles leading to a total of 20000 starting points (1000 voxels in the ROI). After the tracking, the trajectories reaching the thalamus ROI are selected first. Then, these trajectories are split in order to keep only the part linking the two ROIs. A 3D view of the q-balls crossed by the remaining trajectories is proposed in Fig. 5. While the auditory bundle orientation is clear close to Heshl gyrus from the q-ball shapes, the q-balls of the crossing area depict mainly the orthogonal bundle that disturb the streamline approach. A threshold of 3 particles in the density map was used to select further reliable trajectories, which defined a reasonable putative auditory bundle for the three subjects (see Fig. 5).

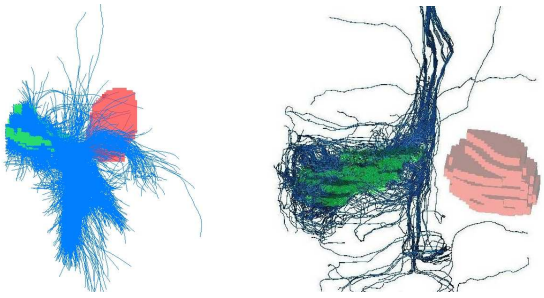

Fig. 6. Left: *the entire set of particle trajectories* **right:** *the equivalent set of streamlines.*

We performed an additional experiment to compare globally the particle trajectories with streamlines computed for the same data and with the same starting points, using a 80 degrees threshold on angles. The results are shown in Fig. 6. The streamlines are all attracted by the orthogonal bundle.

5 Conclusion

In this paper, we have explored the new possibilities provided by q-ball representations for untangling fiber crossing during tracking. We have shown with the phantom study that the additional information on the fiber ODF provided by the q-ball increases largely the potential of tracking algorithms. In this paper, we advocate the use of probabilistic tracking approaches, which can embed uncertainty about the fiber ODF. The potential of this kind of approaches had already been shown in previous work using tensor [4, 3, 5] and multi-tensor models [16]. Here, we have shown that the probabilistic framework fits perfectly the information provided by the q-ball, even if some more work has to be done in order to convert q-ball data into a more reliable fiber ODF. For instance, the proportions of the different fiber orientations included in a voxel influence the q-ball in a way that should be corrected in the fiber ODF. This could largely bias the algorithm described in this paper. This algorithm was kept deliberately simple to prevent the need for sophisticated theoretical development that would be meaningless because of our lack of understanding of the link between the two ODFs. The development of new phantoms could be of great help to improve this understanding. Some of the key parameters whose influence on q-ball should be studied are the proportions of the bundles, the angle between the bundles and the bending of the bundles.

While the experiments with the human brain data may be discussed, because the acquired data are far to optimize the q-ball representation, they show that gathering some of the most advanced ideas of the diffusion community (q-ball, probabilistic tracking, curvature regularization) allows the tracking to get closer to the few a priori anatomical knowledge about the brain connectivity. The next stage will imply to use higher angular resolution data and higher b-value, in order to address the tracking of longer bundles.

References

1. P. J. Basser, J. Mattiello, and D. LeBihan. MR Diffusion Tensor Spectroscopy and Imaging. *Biophysical Journal*, 66:259–267, January 1994.
2. P. J. Basser, S. Pajevic, C. Pierpaoli, J. Duda, and A. Aldroubi. In vivo fiber tractography using DT-MRI data. *MRM*, 44(4):625–32, 2000.
3. T.E.J Behrens, H. Johansen-Berg, M.W Woolrich, S.M.Smith, C.A.M Wheeler-Kingshott, P.A. Boulby, G.J. Barker, E.L. Sillery, K. Sheehan, O. Ciccarelli, A.J. Thompson, J.M. Brady, and P.M. Matthews. Non-invasive mapping of connections between human thalamus and cortex using diffusion imaging. *nature neuroscience*, 6(7):750–7, 2003.
4. T.E.J Behrens, M.W. Woolrich, M. Jenkinson, H. Johansen-Berg, R.G. Nunes, S. Clare, P.M. Matthews, J.M. Brady, and S.M. Smith. Characterization and propagation of uncertainty in diffusion-weighted mr imaging. *Magnetic Resonance in Medicine*, 50:1077–1088, 2003.
5. M. Björnemo, A. Brun, R. Kikinis, and C.-F. Westin. Regularized stochastic white matter tractography using diffusion tensor mri. In *MICCAI'02, LNCS 2488, Springer Verlag*, pages 435–442, 2002.
6. T. E. Conturo, N. F. Lori, T. S. Cull, E. Akbudak, A. Z. Snyder, J. S. Shimony, R. C. McKinstry, H. Burton, and M. E. Raichle. Tracking neuronal fiber pathways in the living human brain. *Proc. Natl. Acad. Sci. USA*, 96:10422–10427, August 1999.
7. L.R Frank. Anisotropy in high angular resolution diffusion-weighted mri. *Magnetic Resonance in Medicine*, 45:935–939, 2001.

8. K.M. Jansons and D.C. Alexander. Persistent angular structure: new insights from diffusion magnetic resonance imaging data. *Inverse Problems*, 19(5):1031–1046, 2003.
9. M. Lazar, J. S. Tsuruda D. Weinstein, K. Arfanakis K. M. Hasan, M. E. Meyerand, B. Badie, H. A. Rowley, V. Haugton, A. Field, and A. Alexander. White matter tractography using diffusion tensor deflection. In *Hum Brain Mapp*, volume 18, pages 306–321, 2003.
10. C. Lenglet, R. Deriche, and O. Faugeras. Inferring white matter geometry from diffusion tensor mri: Application to connectivity mapping. In *8th European Conference on Computer Vision*, 2004.
11. C.M. Leonard, C. Puranik, J. Kuldau, and L.J. Lombardino. Normal variation in the frequency and location of human auditory cortex landmarks. heschl's gyrus: where is it? *Cereb Cortex.*, 8(5):397–406, 1998.
12. C.P Lin, V.J. Wedeen, J.H. Chen, C. Yao, and W.Y.I Tseng. Validation of diffusion spectrum magnetic resonance imaging with manganese-enhanced rat optic tracts and ex vivo phantoms. *NeuroImage*, 2003.
13. J.-F. Mangin, C. Poupon, Y. Cointepas, D. Rivière, D. Papadopoulos-Orfanos, C. A. Clark, J. Régis, and D. Le Bihan. A framework based on spin glass models for the inference of anatomical connectivity from diffusion-weighted MR data. *NMR in Biomedicine*, 15:481–492, 2002.
14. S. Mori, B.J. Crain, V. P. Chacko, and P. C. M. van Zijl. Three dimensional tracking of axonal projections in the brain by magnetic resonance imaging. *Ann. Neurol.*, 45:265–269, 1999.
15. S. Mori and P.C. van Zijl. Fiber tracking: principles and strategies - a technical review. *NMR Biomed*, 15(7-8):468–80, 2002.
16. G. J. M Parker and D. C. Alexander. Probabilistic Monte Carlo based mapping of cerebral connections utilising whole-brain crossing fibre information. In *IPMI, Ambleside*, volume 18, pages 684–95, 2003.
17. C. Poupon, C.A. Clark, V. Frouin, J. Régis, I. Bloch, D. Le Bihan, and J-F. Mangin. Regularization of diffusion-based direction maps for the tracking of brain white matter fascicles. *NeuroImage*, 12(2):184–195, 2000.
18. J. Rademacher, P. Morosan, T. Schormann, A. Schleicher, C. Werner, H-J Freund, and K. Zilles. Probabilistic mapping and volume measurement of human primary auditory cortex. *NeuroImage*, 13:669–683, 2001.
19. E.O Stejskal and T.E Tanner. Spin diffusion measurements: spin echoes in the presence of a time dependent field gradient. *The journal of Chemical Physics*, 42:288–92, 1965.
20. D. S. Tuch. *Diffusion MRI of complex tissue structure*. PhD thesis, MIT, 2002.
21. D. S. Tuch. Q-ball imaging. *Magn Reson Med*, 52(6):1358–72, 2004.
22. D. S. Tuch, T. G. Reese, M. R. Wiegell, N. Makris, J.W. Belliveau, and V. J. Wedeen. High angular resolution diffusion imaging reveals intravoxel white matter fiber heterogeneity. *Magn Reson Med*, 48(4):577–82, 2002.
23. D. S. Tuch, T. G. Reese, M. R. Wiegell, and V. J. Wedeen. Diffusion MRI of complex neural architecture. *Neuron*, 40(5):885–895, 2003.
24. D. S. Tuch, M. R Wiegell, T. G. Reese, J. W. Belliveau, and J Van Wedeen. Measuring corticocortical connectivity matrices with diffusion spectrum imaging. In *ISMRM*, page 502, 2001.
25. J. Van Wedeen, T. G. Reese, D. S. Tuch, M. R. Weigel, J.-G. Dou, R.M. Weiskoff, and D. Chessler. Mapping fiber orientation spectra in cerebral white matter with fourier-transform diffusion. In *ISMRM*, page 82, 2000.
26. David M. Weinstein, Gordon L. Kindlmann, and Eric C. Lundberg. Tensorlines: Advection-diffusion based propagation through diffusion tensor fields. In David Ebert, Markus Gross, and Bernd Hamann, editors, *IEEE Visualization '99*, pages 249–254, San Francisco, 1999.